


# Mechanical Stimulation and Diameter of Fiber Scaffolds Affect the Differentiation of Rabbit Annulus Fibrous Stem Cells

Pinghui Zhou<sup>1,2</sup> · Bangguo Wei<sup>1,2</sup> · Jingjing Guan<sup>1</sup> · Yu Chen<sup>2,3,4</sup> ·  
Yansong Zhu<sup>3</sup> · Yuchen Ye<sup>1</sup> · Yue Meng<sup>1</sup> · Jianzhong Guan<sup>1,2</sup> · Yingji Mao<sup>1,2,3</sup> 

Received: 25 August 2020 / Revised: 12 September 2020 / Accepted: 20 September 2020 / Published online: 3 November 2020  
© The Korean Tissue Engineering and Regenerative Medicine Society 2020

## Abstract

**BACKGROUND:** Degeneration of the annulus fibrosus (AF), an important structure of the intervertebral disc, is one of the main causes of degenerative disc disease. Fabrication of scaffolds replicating the stratified microstructure of the AF is critical for the successful regeneration of AF.

**METHODS:** In this study, we cultured rabbit AF-derived stem cells (AFSCs) using fabricated electrospun fibrous poly-L-lactic acid scaffolds with different diameters. We applied cyclic tensile strain (CTS) on the scaffolds to regulate the differentiation of AFSCs into specific cell types that resided at the inner, middle, and outer zones of the AF.

**RESULTS:** We found that the morphologies of AFSCs on the smaller-fiber-diameter scaffolds were nearly round, whereas spindle-like cells morphologies were observed on large-diameter scaffolds. CTS enhanced these phenomena and made the cells slender. The expression levels of collagen-I in cells increased as a function of the fiber diameter, whereas collagen-II and aggrecan exhibited opposite trends. Moreover, the application of CTS upregulated the gene expressions of collagen-I, collagen-II, and aggrecan.

**CONCLUSION:** Overlaying the scaffolds with different CTS-stimulated cells could eventually lead to engineered AF tissues with hierarchical structures that approximated the native AF tissue. Thus, the proposed methodologies could be potentially applied for AF regeneration.

**Keywords** Intervertebral disc degeneration · Cyclic tensile strain · Poly-L-lactic acid scaffold · Annulus fibrosus-derived stem cells · Differentiation

Pinghui Zhou and Bangguo Wei have contributed equally to this work.

✉ Jianzhong Guan  
jzguan2002@163.com

✉ Yingji Mao  
myj123@bbmc.edu.cn; maoyingji252@yeah.net

<sup>1</sup> Department of Orthopedics, First Affiliated Hospital, Bengbu Medical College, Bengbu 233004, China

<sup>2</sup> Anhui Province Key Laboratory of Tissue Transplantation, Bengbu Medical College, Bengbu 233030, China

<sup>3</sup> School of Life Sciences, Bengbu Medical College, Bengbu 233030, China

<sup>4</sup> Department of Plastic Surgery, the First Affiliated Hospital of Bengbu Medical College, Bengbu 233004, China

## 1 Introduction

Discogenic low back pain (LBP) is one of the most prevalent musculoskeletal conditions. It affects 85% of the adult population at some point during their lifetime and invariably leads to a considerable socioeconomic burden [1, 2]. Approximately 10% of patients are chronically disabled as a result of this condition. As such, LBP decreases the productivity and living quality, while the estimated healthcare expenditures in the United States exceed \$85 billion [3]. The main cause of LBP is intervertebral disc degeneration [4]. Current treatment methods for intervertebral disc degeneration range from nonsurgical therapies used to alleviate intervertebral disc (IVD) pain

and symptoms following operative treatments, including discectomy, spinal fusion, and total disc replacement [5]. However, these surgical strategies fail to restore disc function and often lead to degeneration of adjacent disc levels [6–8].

The intervertebral disc comprises three integrated structures, the inner gelatinous nucleus pulposus (NP), the outer collagen-rich annulus fibrosus (AF), and the avascular and aneural cartilage endplate that connects the intervertebral disc to the vertebral bodies [9]. Its main function is to absorb and distribute compressive loading and lend flexibility to the spine [10]. The integrity of the AF, an important structure of the IVD, plays a critical role in maintaining its structure and function [11, 12]. The AF is a heterogeneous tissue that can be divided into three zones from its inner to outer parts along the radial direction. Accordingly, the cell type, matrix composition, microstructure, and mechanical properties of each zone exhibit typical gradient changes [11]. The matrix of the AF is mainly composed of 15 to 25 concentric sheets of inner collagen type II with small diameters and outer collagen type I with large diameters [13]. This particular structure maintains the stability of the IVD when subjected to long-term mechanical loads [14]. The NP tissue breaks through one or more of these already weakened and oriented tissues and may result in the onset of degenerative disc disease, such as LBP, and limited mobility of the spine [15–17].

Tissue engineering technologies mimicking native IVD, such as NP regeneration, AF repair, and NP–AF composite replacement, maybe a promising strategy for the restoration of the structure and the improvement of the function of IVD [18]. Owing to its biocompatibility, low antigenicity, low cytotoxicity, processability, and biodegradability, poly(L-lactide) (PLLA) is a good scaffold material candidate and has been extensively used in various biomedical fields, such as tissue engineering and regenerative medicine, for the repair and reconstruction of ligaments and drug-eluting stents [19, 20]. Studies have shown that PLLA-based biomaterials, alone, or in combination with a second constituent, such as chitosan, hydrogel, or polycaprolactone, can maintain the mesenchymal stem cell phenotype, and the capacity of these cells to proliferate and differentiate [23, 24]. Existing evidence suggests that the PLLA-based scaffolds constitute promising materials as cell repositories adjacent to damaged discs. The study by Valada et al. (2012) developed a bioactive PLLA scaffold with transforming growth factor- $\beta$ 1 for the repair and regeneration of damaged AF. However, the anisotropic nanofibers of the native AF had not been replicated. Accordingly, this may ultimately lead to the degeneration of tissue-engineered IVD in vivo [25].

Mechanical loads, including compressive pressure, tensile strain, fluid flow, and hydrostatic pressure, are crucial

for maintaining physiological conditions for IVD [26, 27]. Physiological and nonphysiological mechanical stimulation can lead to the anabolism and catabolism, respectively, of the extracellular matrix. For example, a study found that appropriate mechanical stimulation increased the synthesis of collagen and glycosaminoglycan [28]. Moreover, another experiment found that excess mechanical loads decreased the expressions of anabolic genes [29]. Consequently, changes in the extracellular matrix can modify the biomechanics of an intervertebral disc. Therefore, it is important to use a moderate mechanical load for IVD.

Whether the mechanical stimuli and the microstructure of the aligned PLLA fibers with different diameters influence the structural and functional integrity of the IVD. We have reported previously that PLLA fibrous scaffolds with fiber diameters in the range of 0.52–3.23  $\mu$ m could effectively regulate the differentiation of AFSCs to the specific cell types contained in the native AF [30]. Therefore, the objective of the present study is to investigate the influences of PLLA fibers diameters (11, 15, and 25 wt %) and cyclic tensile strain (5% strain magnitude, 0.5 Hz) on AFSCs in vitro (Fig. 1). To investigate the possible interactions of both factors on the AF structure, cell viability, morphology, and the expression levels of messenger ribonucleic acid (mRNA) of anabolic genes were assessed. The aim was to fabricate and analyze a tissue-engineered AF with mechanical and structural simulation in vitro that could be applied for AF regeneration in vivo.

## 2 Materials and methods

### 2.1 Fabrication of aligned PLLA scaffolds with different diameters

PLLA fibers were fabricated through electrospinning, as described previously [11, 31]. Briefly, polymer solutions were prepared by dissolving 0.75 g, 1 g, and 2 g PLLA in 2 g N, N-dimethylformamide, and 4 g dichloromethane (DCM), respectively, at the concentrations of 11, 15, and 25% (w/w), respectively, to fabricate small fibers (small-F), medium fibers (medium-F), and large (large-F) fibers. The prepared polymer solutions were used to load 5 mL plastic syringes (with 18 G needles), and their contents were released in a controlled manner at feeding rates in the range of 10–50  $\mu$ L/min with a syringe pump (Longer Pump Co., Ltd., Baoding, Hebei, China). The high-voltage-power supply (Tianjin High Voltage–Power Supply Co., Ltd., Tianjin, China) maintained the voltage within the range of 10–15 kV. The distance between spinneret and collector was set at 15 cm. The rotating disk was applied as the collector of the electrospun fibers, and the rotation speed of the collector was set to 2000 revolutions per

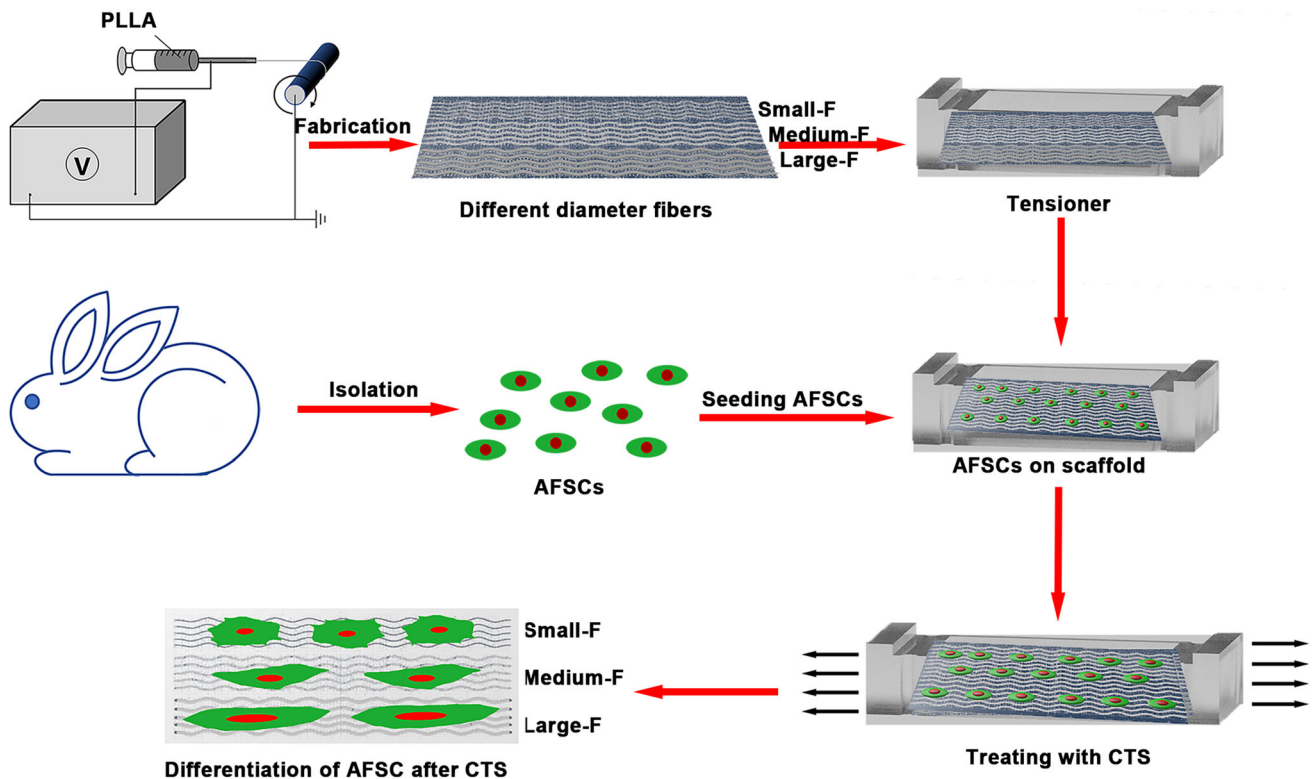


**Fig. 1** Schematic illustration of the poly-L-lactic acid (PLLA) based gradient diameter of electrospun fibrous with cyclic tensile strain (CTS) affects the differentiation of rabbit annulus fibrosus stem cells

minute for fabricating aligned PLLA scaffolds. Control of the spraying time helped maintain the thickness of different fiber diameter scaffolds the same. In brief, measuring the thickness with a Vernier caliper, we fabricated the fibrous membrane and stopped when the thickness at 0.13 mm. The resulting scaffolds were dried in the presence of a vacuum overnight and stored at  $-20\text{ }^{\circ}\text{C}$  for subsequent experimental use.

## 2.2 Physicochemical and mechanical characterization of scaffolds

Scanning electron microscopy (SEM, S-4800, Hitachi Co. Ltd., Kyoto, Japan) was used to observe the morphology and microstructure of aligned PLLA scaffolds with different diameters. The software ImageJ was used for analysis of the diameter distribution of 50 fibers in each sample. The hydrophobicity and hydrophilicity of the scaffolds was measured using a contact angle measuring system (DSA25, KRÜSS, Hamburg, Germany) through the sessile drop-shape method. In this method, a drop of distilled water was placed on the surface of the scaffolds to conduct contact angle measurements at  $25\text{ }^{\circ}\text{C}$ . To assess the mechanical properties of the fabricated scaffolds, the fibrous membrane specimens were cut into cuboids (sizes of  $15.0 \times 3.0 \times 0.13\text{ mm}^3$ ) and placed on a tensile testing

machine (Instron 3365, Norwood, MA, USA). The uniaxial tensile measurements were performed at a tensile rate of  $5\text{ mm/min}$ . All experiments were repeated three times.

## 2.3 Preparation of PDMS sheets

The PDMS sheets were cast with a silicon resin (ELASTOSIL1 RT601, Wacker Chemical, Adrian, MI, USA). The silicon resin was composed of components A and B, which were mixed at a ratio of 10:1, and then poured in chamber molds for 3 days to fabricate the PDMS sheets. The appropriate size of the PLLA scaffolds were glued to the bottom of the PDMS dishes with biological glue, and the samples were then treated in a plasma treatment device for 5 min, then sterilized with ultraviolet (UV) radiation, subsequently, and were soaked in the medium for 4 h in the humidified incubator at  $37\text{ }^{\circ}\text{C}$  with  $5\%\text{ CO}_2$ . Finally, these were washed with phosphate buffer solution (PBS) three times, followed by drying, before the cells were seeded.

## 2.4 Isolation and differentiation of rabbit AFSCs

The animal surgery protocols were approved by the Institutional Animal Care and Use Committee (IACUC) of Soochow University. Rabbit AFSCs were isolated, cultured, and characterized as previously described [32, 33].

Briefly, AFSCs were obtained from New Zealand white rabbits (4–6 weeks old) in sterile conditions. The tissue was sectioned in 1 mm<sup>3</sup> cuboid and was then digested in low-glucose Dulbecco's modified eagle medium (DMEM-LG, SH30021.01B; Hyclone, Thermo Fisher Scientific, Hudson, NH, USA) with collagenase I (150 U/ml) and collagenase II (150 U/ml) for 2–4 h. Finally, AFSCs were collected and cultured in the DMEM-LG medium with 15% fetal bovine serum, 100 U/ml penicillin, and 100 µg/ml streptomycin. Cells were maintained in the humidified incubator at 37 °C with 5% CO<sub>2</sub> and fed with fresh medium every 2 days. The cells were harvested for use in this study after the second passage.

The adipogenesis, osteogenesis, and chondrogenesis of AFSCs were examined using Alizarin Red S, Safranin O, and Oil Red O assay respectively, as previously described [32, 33]. In brief, after the cells reached appropriate confluence, the culture medium was changed into osteogenic, chondrogenic, and adipogenic medium, respectively. Subsequently, the cells were stained with Alizarin Red S, Safranin O, and Oil Red O solution after fixed in 4% paraformaldehyde at specific time. The samples were observed under an inverted microscope (Carl Zeiss Inc., Thornwood, NY, USA).

## 2.5 Cell seeding and viability

Before cell culturing, the PDMS chambers coated with PLLA scaffolds were cut into rounded samples that fit the 96-well cell culture plates, then sterilized with UV radiation and washed with PBS at least three times. Subsequently, the AFSCs were seeded on PLLA scaffolds at a density of  $5 \times 10^3$  cells/well in the DMEM-LG medium. The samples were incubated in a humidified incubator at 37 °C with 5% CO<sub>2</sub> for different periods (1, 3, 5, and 7 days), and the cell culture medium was refreshed every 2 days. Cell viability was monitored with an MTS assay (CellTiter 96 Aqueous, Promega, Madison, WI, USA). The cells were washed two times with PBS at the indicated periods, followed by incubation with 10% MTS reagent in DMEM-LG at 37 °C for 3 h. Finally, the absorption of the solution was measured by a microplate reader (BioTek Instruments, Winooski, VT, USA) at a wavelength of 490 nm. All experiments were repeated for three times.

## 2.6 Application of cyclic tensile strain

The PLLA scaffolds were cut into rectangular shapes and spread out on the elastic silicone dish with PDMS. They were then sterilized and washed with PBS at least three times. Subsequently, the AFSCs were seeded on PLLA scaffolds at a density of  $2 \times 10^6$  cells/sheet in the DMEM-LG medium. When the cells reached 70% confluence, the

cell-scaffold chambers were randomly divided into experimental and control groups. AFSCs were subjected to CTS with 5% strain magnitude at 0.5 Hz for 4 h/day with the Flexercell 4000T Tension Plus strain unit (Flexercell, McKeesport, PA, USA) which generated uniform radial and circular strain across the membrane surface. The cells in the control groups were cultured without CTS stimulation. They were then maintained in a humidified incubator at 37 °C with 5% CO<sub>2</sub> for 3 days.

## 2.7 Morphological analyses

For the staining of the cytoskeleton, the AFSCs seeded on scaffolds (with or without CTS) were rinsed twice with PBS after 7 days, fixed with 4% paraformaldehyde for 15 min, and permeabilized with 0.1% Triton X-100 for 5 min. After incubation with 10% bovine serum albumin blocking in PBS, the cells were stained with fluorescein isothiocyanate-phalloidin (1:300 v:v, Enzo Biochem, New York, NY, USA) in PBS for 40 min in the presence of light-protection conditions to identify filamentous actin. Cells were then washed three times with PBS for 5 min, followed by incubation with 4'6'-diamidino-2-phenylindole (1:300 v:v, Roche, Basel, Switzerland) in PBS for 10 min, which was applied to stain nuclei. After three washes with PBS for 5 min, the cells were visualized with a fluorescence microscope (Zeiss Axiovert 200, Carl Zeiss Inc, Thornwood, NY, USA). The cell spreading area and shape index were semi-quantitated using ImageJ. Three equivalent images were randomly selected from each group.

For SEM observations, the cells on the scaffolds were rinsed with PBS twice and subsequently fixed using 2.5% glutaraldehyde for 2 h. The samples were dehydrated with graded ethanol (concentrations from 10% to 100%) for 15 min, followed by critical-point drying and sputter-coating with gold. Imaging was photographed at an accelerating voltage of 4 kV.

## 2.8 RNA isolation and quantitative reverse transcription-polymerase chain reaction (RT-qPCR)

After 7 days in culture, RT-qPCR was employed to examine the mRNA expression level of AF related genes (collagen-I, collagen-II, and aggrecan) on the scaffold after CTS treatment. The AFSCs were digested with 0.25% trypsin, and the total RNA was isolated using a TRIZOL isolation system (Invitrogen, Thermo Fisher Scientific, Hudson, NH, USA), according to the manufacturer's protocol. Complementary deoxyribonucleic acid was reversely transcribed by the RT-qPCR system (Eastwin Life Science, Beijing, China). Glutaryldehyde 3-phosphate dehydrogenase (GAPDH) was used as the reference gene. All the

specific primers used in this study are listed in Table 1. RT-qPCR was performed with the SsoFast EvaGreen Supermix Kit (Bio-Rad, Berkeley, CA, USA). The relative expression levels of the genes were calculated with the  $2^{-\Delta\Delta Ct}$  method after GAPDH standardization. Three biological repeats and technical repeats were applied for each gene.

## 2.9 Biochemical assays

After 7 days of culture, the supernatants of cells cultured on the scaffolds were harvested. The levels of collagen-I and collagen-II were examined using enzyme-linked immunosorbent assay (ELISA) kits (R&D Systems, Minneapolis, MN, USA). The content of glycosaminoglycan (GAG) was quantified with the 1, 9-dimethylmethylene blue dye-binding assays with a commercially available kit (Genmed Scientifics Inc., San Antonio, TX, USA, GMS 19239.2). The deoxyribonucleic acid (DNA) production was determined by the DNA-binding fluorochrome Hoechst 33258 dye (Sigma, St. Louis, MO, USA) applied for 30 min in dark conditions. The GAG production was normalized to the corresponding DNA content. All experiments were repeated for three times.

## 2.10 Statistical analysis

All data were presented as means  $\pm$  standard deviations (SD) and analyzed using the SPSS 18.0 software (Chicago, IL, USA). Comparisons between groups were evaluated using Kruskal–Wallis one-way analysis of variance, followed by Tukey post hoc tests. The value of  $p < 0.05$  was considered significant for all tests.

## 3 Results

### 3.1 Characterizations of aligned PLLA scaffolds and AFSCs

The aligned PLLA fibers with different fiber diameters and highly porous three-dimensional structures were fabricated

with electrospinning. We varied the rotating speed of the rotating pan to control the orientation of the fibers and changed the content of PLLA in the solution to obtain scaffolds with different fiber diameters. After formation, the characterization of the scaffolds was determined by SEM and uniaxial tensile tests. As the hydrophilicity of the materials played a crucial role in cell cultures, we examined the static water contact angles of PLLA fibrous membranes (Fig. 2).

The results showed that the concentration of the PLLA solution significantly influenced the fiber diameter and morphology (Fig. 2A). With the increase of the concentration from 11 to 25%, the fiber diameter increased from  $0.52 \pm 0.09 \mu\text{m}$  to  $3.23 \pm 0.21 \mu\text{m}$  (Fig. 2A). Otherwise, the tensile strengths of the PLLA membranes increased from  $1.17 \pm 0.20$  to  $1.98 \pm 0.32 \text{ MPa}$  (Fig. 2B). The breaking elongations of the membranes, however, decreased from  $52.68 \pm 0.49$  to  $27.67 \pm 0.64\%$  (Fig. 2B). Interestingly, the water contact angles of scaffolds were approximately  $135^\circ$  and did not vary when the fiber diameter changed (Fig. 2C). Therefore, the strength of the scaffolds was found to increase as a function of the fiber diameter of the scaffolds, whereas the tensile moduli of the membranes were found to be similar.

As showed in Fig. 3, both the mineralization, cartilage matrix and secretion of oil droplets were increased after cultured in inducing and differentiation medium, indicating the cells we isolated have stem cell properties for osteogenic, chondrogenic and adipogenic differentiation (Fig. 3A, B, and C).

### 3.2 Viability of AFSCs

To evaluate the viability of CTS-treated or CTS-untreated AFSCs on the different diameter scaffolds, we conducted the MTS assays at specific time intervals (1, 3, 5, and 7 days) (Fig. 3D and E). The results showed that mechanically unstimulated AFSCs exhibited good viability on all the scaffolds. The same results were observed for the stimulated AFSCs. In addition, there were no significant differences among the AFSCs cultured on the scaffolds with loading or unloading CTS on the same day. Therefore,

**Table 1** Quantitative RT-PCR primer sequences

Gene	Forward primer (5'-3')	Reverse primer (5'-3')	Accession number
GAPDH	ACTTTGTGAAGCTCATTTCCTGGTA	GTGGTTTGAGGGCTCTTACTCCTT	NM_001082253
Collagen-I	CTGACTGGAAGAGCGGAGAGTAC	CCATGTGCGAGAAGACCTTGA	AY633663
Collagen-II	AGCCACCCTCGGACTCT	TTCCTGCCTCTGCCTG	NM_001195671
Aggrecan	ATGGCTTCCACCAAGTGGC	CGGATGCCGTAGGTTCTCA	XM_002723376

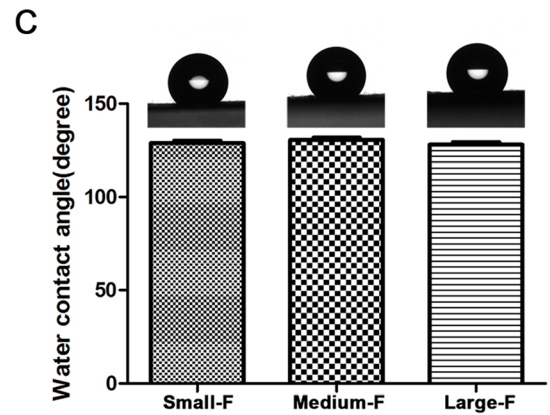
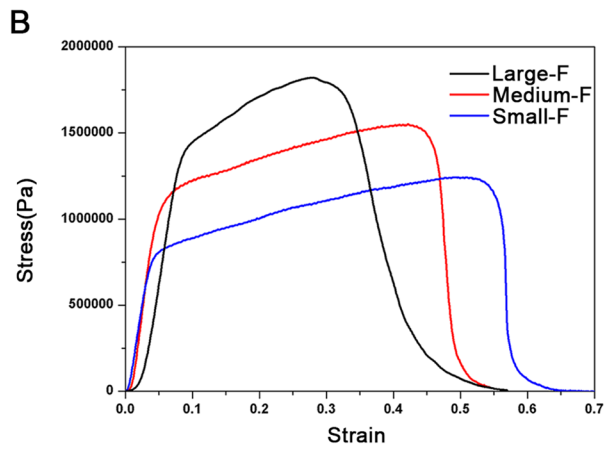
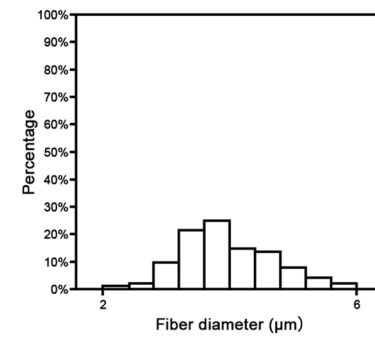
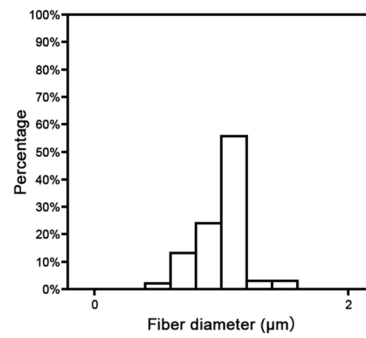
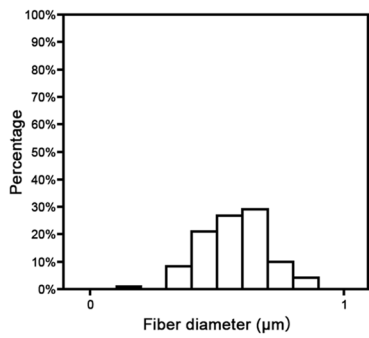
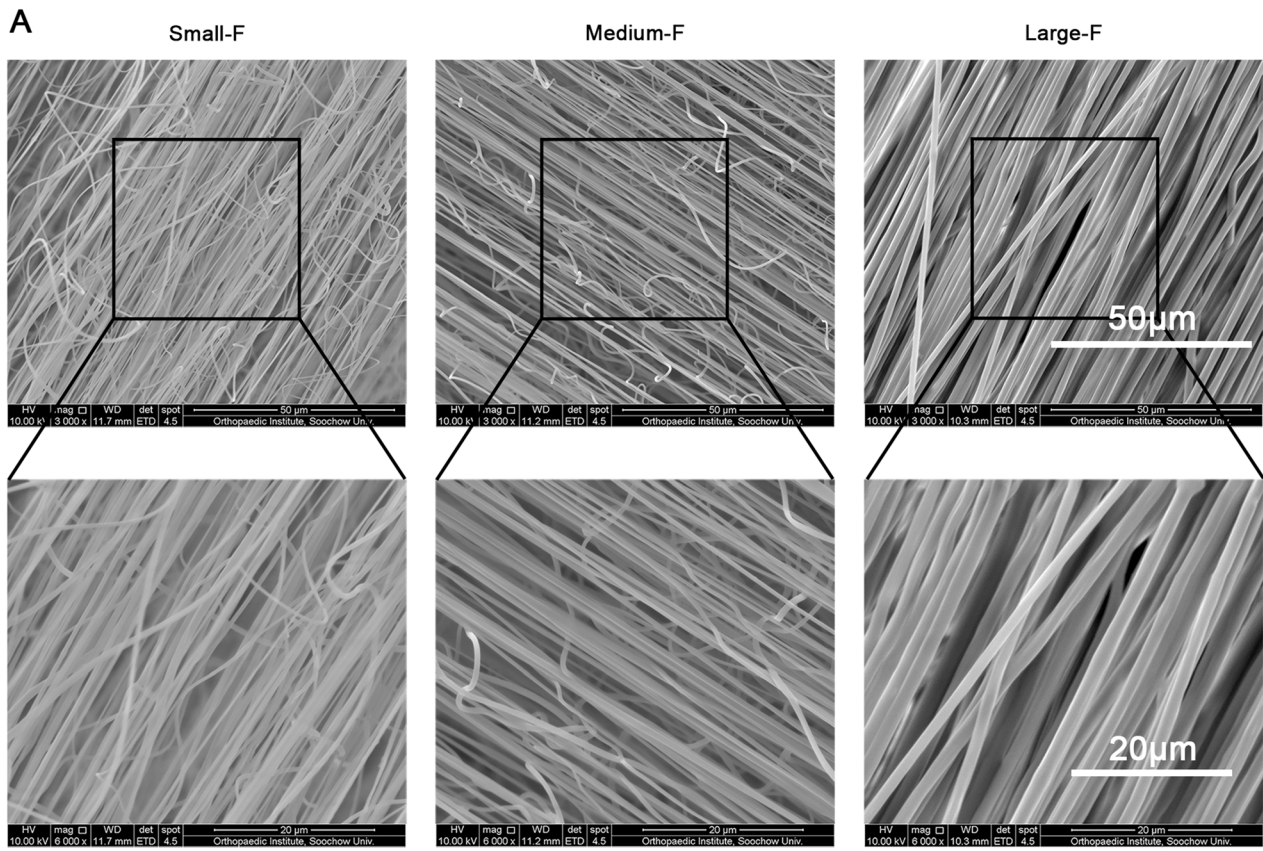


**Fig. 2** Characterization of the scaffolds. **A** Different fiber diameter of electrospinning membranes with different PLLA content under SEM and the fiber diameter were examined quantitatively. **B** The tensile strengths of scaffolds with stress–strain test. **C** The water contact angle of the scaffolds. Data are presented as mean ( $n = 3$ )  $\pm$  SD

good viability were noted for AFSCs on all the scaffolds. This indicated that the scaffolds yielded no obvious

cytotoxic effects and could support suitable environments for cell viability, while the CTS did not significantly affect the viability of the AFSCs.

### 3.3 Morphology of AFSCs

To visualize the morphology of CTS stimulated and unstimulated AFSCs on scaffolds with different diameter

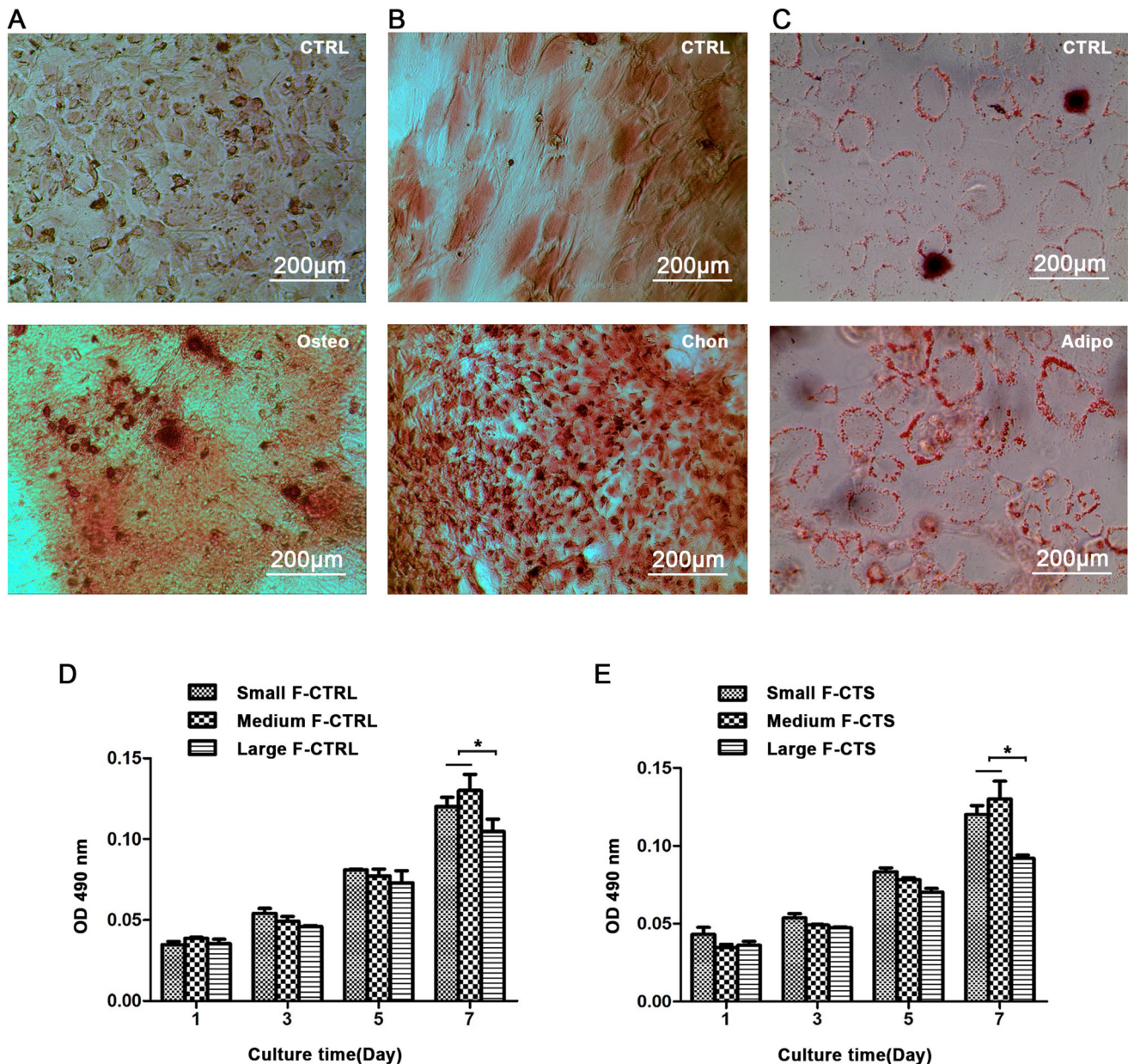


**Fig. 3** Induced differentiation of AFSCs. **A** Osteogenic differentiation: mineralization is visualized using Alizarin red S solution after 21 days culture in osteogenic medium. **B** Chondrogenic differentiation: cartilage matrix is stained with Safranin O solution after 21 days culture in chondrogenic medium. **C** Adipogenic differentiation: oil droplets are stained using the Oil Red O solution after 14 days of

culture in an adipogenic medium. The isolated AFSCs have stem cell properties for osteogenic, chondrogenic, and adipogenic differentiation. The viability of AFSCs **D** without CTS and **E** with CTS on the scaffolds by MTS assays. CTS did not affect the cell viability. Data are presented as mean ( $n = 3$ )  $\pm$  SD. \*,  $p < 0.05$

fibers, we conducted fluorescein isothiocyanate-phalloidin and 4'6'-diamidino-2-phenylindole staining for actin cytoskeleton (green) and cell nuclei (blue), respectively (Fig. 4A and B). The micrographs of phalloidin staining showed that AFSCs attached to all the scaffolds irrespective of the microstructures and CTS. However, they displayed distinct morphologies on different scaffolds between (control and CTS group).

The morphologies of unstimulated AFSCs cultured on scaffolds with small diameters were nearly round in shape, and their actin filaments were extended in random directions. By contrast, for scaffolds made with large-diameter fibers, elongated cell morphologies were observed, and

spindle shapes with their actin filaments extended parallel to the direction of the electrospun fibers (Fig. 4A). The CTS-treated AFSCs cultured on the different diameter scaffolds exhibited similar results. The CTS-stimulated AFSCs, however, were more elongated compared with the unstimulated AFSCs on the same fiber diameter (Fig. 4B). These results were further confirmed by the semi-quantitative analysis of cell spreading area and shape index (the ratio of cellular width to length) (Fig. 4C and D).

The morphologies of the AFSCs were also assessed using SEM (Fig. 4E and F). The SEM images revealed that the seeded AFSCs were attached on the surfaces of fibrous scaffolds and spread along the axial direction of the PLLA

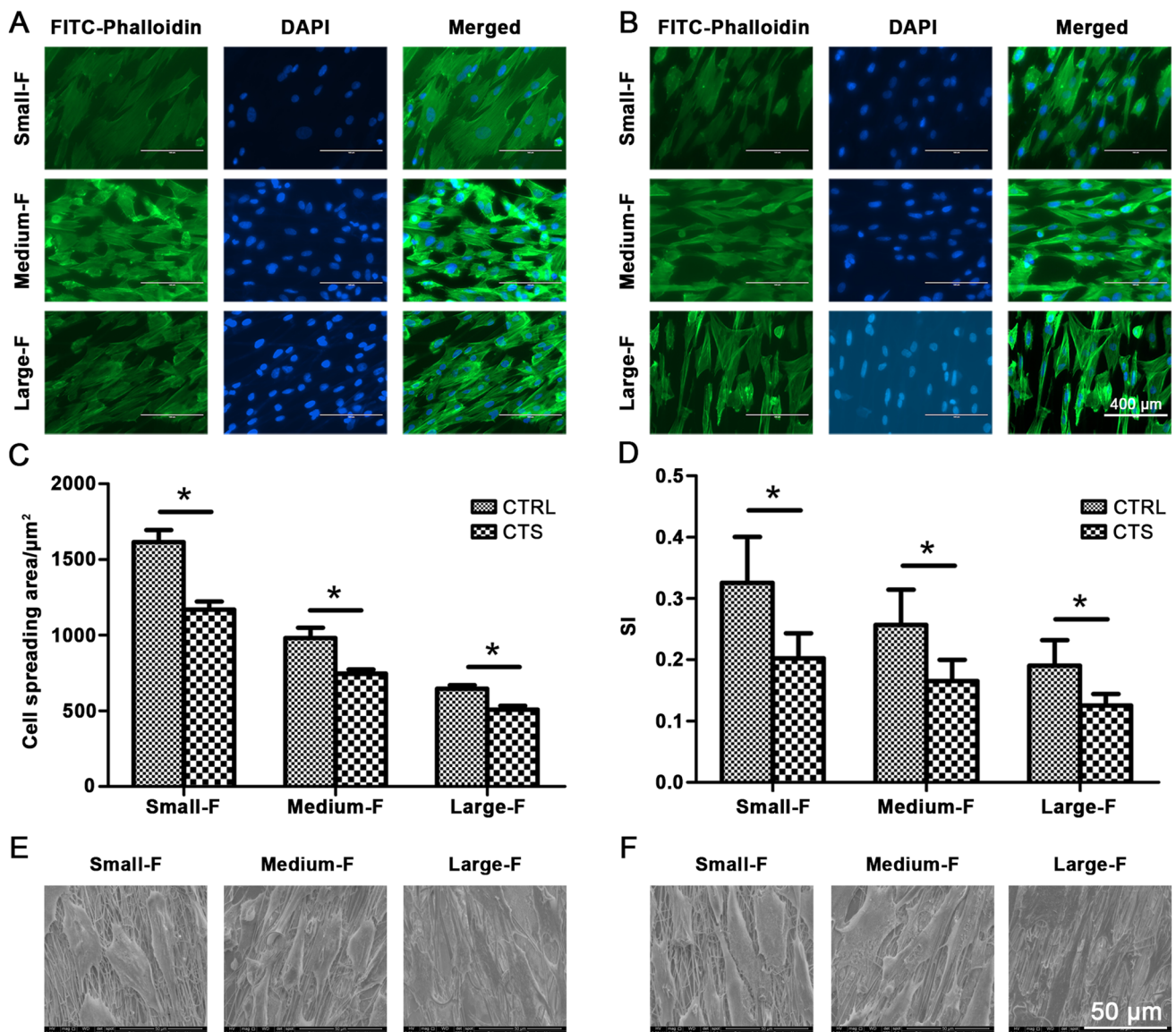


**Fig. 4** The Cytoskeleton staining of AFSCs on PLLA electrospinning membranes of different diameters **A** without CTS and **B** with CTS. DAPI staining for cell nuclei (blue), FITC-Phalloidin staining for actin cytoskeleton (green). And quantitative analysis of **C** cell

spreading area and **D** shape index. **E** SEM of AFSCs on PLLA electrospinning membranes of different diameters **A** without CTS and **B** with CTS. CTS made the cells more slender. Data are presented as mean ( $n = 3$ )  $\pm$  SD. \*,  $p < 0.05$



microfibers. The AFSCs cultured on the scaffolds with small-diameter fibers had polygonal phenotypes irrespective of CTS stimulation, while those on the larger-diameter fibers were spindle-like (Fig. 4E). The CTS-stimulated AFSCs were more spindle-like and there were fewer protrusions compared with the unstimulated AFSCs on the same fiber diameter (Fig. 4F). Therefore, mechanical stimulation of AFSCs with 5% strain at the frequency of 0.5 Hz for 4 h/day and fibers with large diameters resulted in morphological changes that led to the more elongated AFSC phenotypes.

### 3.4 Gene expression of AFSCs

To investigate the stimulating effects of CTS and fiber diameters on the AFSCs, we analyzed the gene expressions of collagen-I, collagen-II, and aggrecan by RT-qPCR, which were the major matrix components of AF (Fig. 5A). The gene expression of collagen-I in unstimulated AFSCs increased as a function of the fiber diameter. Opposite trends were observed for collagen-II and aggrecan. These trends were similar to CTS-stimulated AFSCs. Notably, the gene expression of collagen-I, collagen-II, and aggrecan in all CTS-treated AFSCs were higher than untreated AFSCs cultured on scaffolds with the same diameters. Therefore, the use of stimulated CTS with 5% strain at a frequency of

0.5 Hz for 4 h/day could significantly upregulate the gene expression of collagen-I and collagen-II.

### 3.5 Biochemical contents of AFSCs

Additionally, the abilities of mechanically stimulated and unstimulated AFSCs cultured on scaffolds with different diameters that affected the secretion of matrix components were evaluated by ELISA (Fig. 5B). The content of collagen-I in AFSCs without CTS was observed to increase for small-F, medium-F, and large-F scaffolds by  $5.31 \pm 0.39$ ,  $6.13 \pm 1.11$ , and  $12.29 \pm 1.27$  ng/ $\mu$ g, respectively. The respective contents of collagen-II were measured to be  $8.12 \pm 0.31$ ,  $7.26 \pm 0.37$ , and  $4.72 \pm 0.69$  ng/ $\mu$ g at increasing fiber diameters, and  $12.73 \pm 0.64$ ,  $12.46 \pm 0.11$ , and  $6.64 \pm 0.64$  ng/ $\mu$ g for GAG. These values were consistent with the gene expression outcomes. There were no obvious differences in the contents of collagen-I and collagen-II in the AFSCs on large-F diameter scaffolds and the content of GAG in the control and CTS groups. The contents of collagen-I in CTS-treated AFSCs were measured to be  $7.30 \pm 0.67$ ,  $8.82 \pm 0.12$ , and  $12.63 \pm 1.23$  ng/ $\mu$ g for the three types of scaffolds at increasing fiber diameters. The corresponding contents of collagen-II and GAG were measured to be  $9.59 \pm 0.56$ ,  $9.12 \pm 0.35$ , and  $4.69 \pm 0.47$  ng/ $\mu$ g, and  $12.46 \pm 0.25$ ,  $12.34 \pm 0.61$ , and  $6.91 \pm 0.82$  ng/ $\mu$ g,

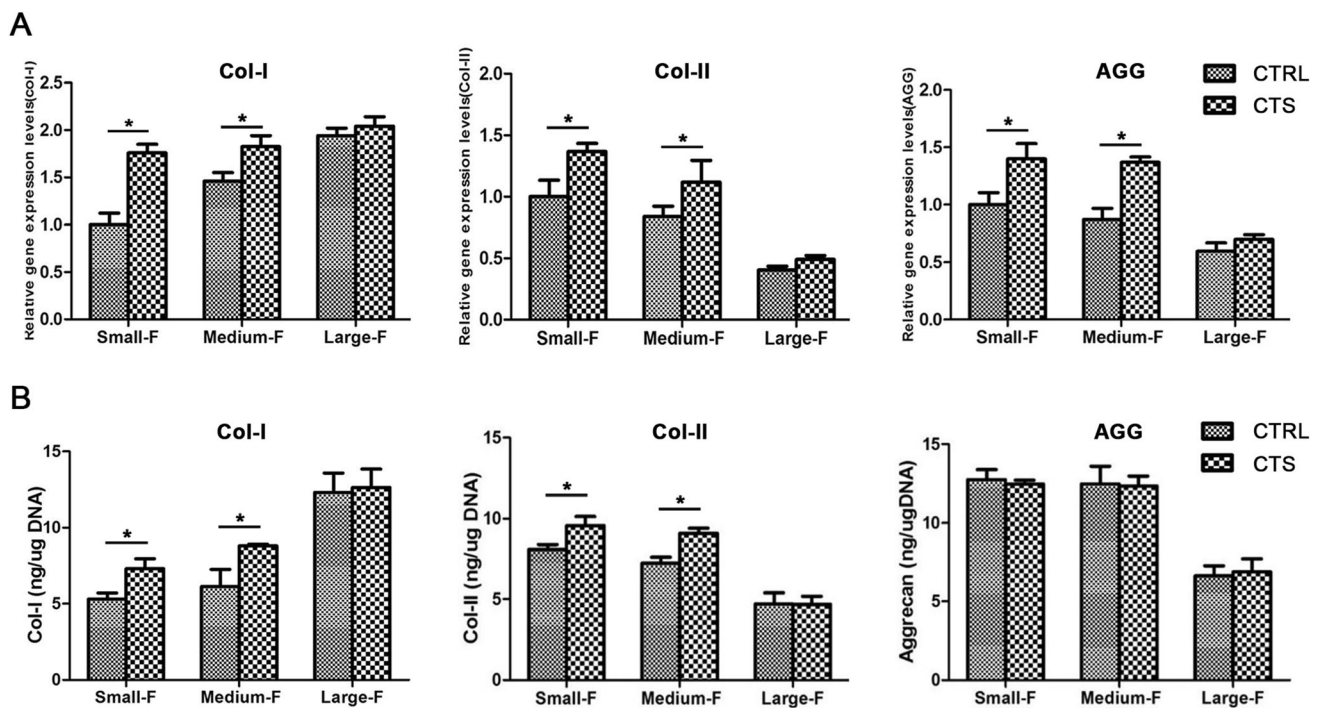


**Fig. 5** RT-qPCR and ELISA of AFSCs on different scaffolds without and with CTS. **A** The application of CTS increased the mRNA expression of gene Col-I, Col-II, and Aggrecan of AFSCs on Small-F

and Medium-F. **B** CTS upregulated the protein expressions of gene Col-I and Col-II on Small-F and Medium-F. Data are presented as mean ( $n = 3$ )  $\pm$  SD. \*,  $p < 0.05$

respectively. Therefore, the application of CTS with 5% strain at 0.5 Hz for 4 h/day increased the content of collagen-I and collagen-II in the AFSCs cultured with small-F and medium-F diameter scaffolds compared with the unstimulated AFSCs on scaffolds with the same diameters.

#### 4 Discussion

The native AF is a heterogeneous tissue composed of three regions along the radial axis. In addition, the inner region is high in collagen type II fibers with small diameters, while the outer is high in collagen type I fibers with large diameters. This complex structure gives the spine the ability to resist the highly complex mechanical loads. Therefore, it is crucial to mimic the morphological conditions of the IVD with the complex hierarchical structure of the AF for tissue regeneration. To investigate the differentiation of AFSCs in response to the fiber diameter of scaffolds and mechanical stimulation, we fabricated aligned fibrous scaffolds with different diameters mimicking the hierarchical structures of the inner, middle, and outer regions of the native AF. The cultured AFSCs were differentiated toward the cell types that corresponded to those at different regions of the AF. When the AFSCs were treated on scaffolds with different diameters with CTS, the morphologies of the AFSCs became extremely similar to the native AF. Finally, the fabricated and engineered AF tissue replicated the anatomical features of native AF by differentiation of AFSC on microstructure scaffolds and mechanical load *in vitro*.

The AF cells of the spine were exposed to CTS during exercise. Mechanical stimulation in the form of CTS is an essential factor to emulate physiological conditions for the IVD. The healthy AF tissues were exposed to strains of ~ 6% along the fiber direction [17]. Various research studies showed that the physiological magnitude, frequency, and duration of CTS could significantly affect the behaviors and the differentiation of AF cells [19, 27, 29]. Hee et al. reported that 10% CTS can upregulate collagen and GAG gene expression [28]. In this study, we found that CTS with 5% strain magnitude at a frequency of 0.5 Hz for 4 h/day could achieve the desired effect. Gilbert et al. found that CTS at high frequency decreased the anabolic gene expression, whereas the catabolic gene expression was increased at a low frequency [29]. Hence, we chose CTS with a strain magnitude of 5% at a frequency of 0.5 Hz for 4 h/day in our study. In our previous study, we found that Caveolin-1 and Yes-associated protein related to cell mechanical signal pathways had significantly transformed after 3 days of mechanical stimulation that indicated that the AFSCs already possessed of the required differentiation cues [34]. Additionally, after 7 days, the

gene expression was significantly different; this suggested that the AFSCs had differentiated. Therefore, we choose 7 days as the time point for the morphology, gene expression, and biochemical assay.

The MTS assays demonstrated that good AFSCs viability was achieved on all the scaffolds irrespective of the fiber diameter. The viability of AFSCs decreased as the fibers diameters increased. This is in accordance with the findings of our previous studies that have reported that this may be attributed to the decrease of the surface area and interstitial space [30]. Additionally, it was demonstrated that the differences in the viability of the cells between the CTS and control groups were negligible (Fig. 3D and E). It has also been shown that mechanical stimulation (type, magnitude, frequency, and duration) can affect the behaviors of cells [4, 35, 36]. For instance, Shradhanjali et al. reported that equiaxial stretch (12% strain, 1.25 Hz, 24 h) could induce P19-derived embryoid body differentiation in spontaneously beating cardiomyocytes [37]. Tomlinson et al. found that axial compression (3.0 N, 0.1 Hz, 100 cycles/day) could upregulate the expression of the nerve growth factor that would, in turn, activate the nerve growth factor-tropomyosin receptor kinase A signaling pathway of skeletal sensory nerves [38]. Chen et al. showed that CTS (10% amplitude, 1 Hz, 2 h daily) could increase the microRNA (miR)-365 expression to induce bone marrow stromal cell chondrogenesis [39]. The morphology of AFSCs was also investigated (Fig. 4). In this study, the AFSCs on the scaffolds with large-F diameters had spindle-like morphologies, whereas cells on those with small-F diameters were relatively round. These findings are consistent with previous findings that showed that the diameters of scaffolds could affect the morphologies of AF cells [15]. We also found that the CTS-stimulated AFSCs were more elongated than those in scaffolds in the control groups with the same diameters. This observation was consistent with data that showed that CTS could stretch the AF cells [17, 26].

To understand the molecular mechanism, based on which the diameter of the scaffolds and CTS interfered with the differentiation of AFSCs, we detected the expressions of collagen-I, collagen-II, and aggrecan, which have been considered as the characteristic matrix molecules of AF tissue (Fig. 5). We found that the gene expression of collagen-I in AFSCs increased as a function of the scaffold diameter. By contrast, the gene expression of collagen-II and aggrecan decreased as the diameter of the scaffolds decreased. In general, the gene expressions of collagen-I, collagen-II, and aggrecan exhibited opposite behaviors when AFSCs were cultured on the scaffolds with large-F diameters. We also found that the gene expression of CTS-treated AFSCs were higher than those of CTS-untreated AFSCs, even though the gene expression

differences of AFSCs cultured on the large-F diameter scaffolds were not statistically significant. This phenomenon was also reported in previous studies. Li et al. found that 10% CTS could upregulate type I and II collagen mRNA levels of the outer AF [26]. Hee et al. reported that 5% tensile strain had no effects on the collagen of human inner AF cells, while 10% tensile strain increased collagen and GAG based on the expansion of the endoplasmic reticulum [28]. These findings may be attributed to the fact that the 5% CTS was too small to sufficiently deform the large-F PLLA scaffolds. Moreover, ELISA revealed that the protein contents of collagen-I and collagen-II yielded similar outcomes to those obtained for gene expression. However, the aggrecan levels were the same in the control and CTS groups. In addition to gene expression, proteases, such as aggrecanases, also determine the total content of aggrecan [1, 38, 39]. This finding is probably attributed to an adaptive response, whereby the aggrecan was degraded by an increasing number of proteases.

In summary, we have successfully fabricated the AF scaffolds with electrospinning technology. Fabricated scaffolds with various diameters were used to emulate the microstructure of the native AF tissue. The morphologies of AFSCs cultured on scaffolds with small diameters were nearly round, and the actin filaments extended in random directions. By contrast, the electrospun fibers with larger diameters were elongated and spindle shaped, and their actin filaments extended in parallel directions. Notably, the CTS with 5% strain at a frequency of 0.5 Hz for 4 h/day enhanced these phenomena and made the AFSCs slender. The expression levels of collagen-I in AFSCs increased with the fiber diameter, while collagen-II and aggrecan showed opposite trends. Moreover, the CTS had upregulated the gene expression patterns of collagen-I, collagen-II, and aggrecan. The main challenge associated with the tissue engineering of biomimetic AF scaffolds is the replication of the three-dimensional hierarchical architecture of the native AF tissue at the cellular and molecular levels. Further studies should fabricate scaffolds with a circumferential fiber with different diameters and anticipate mechanical loading to mimic the hierarchical structures of native AF tissue, which could apply this construct in a large animal model to test the functional outcomes. The present study established the basis for AF tissue engineering through the regulation of the differentiation of AFSCs as a function of the fiber diameters and mechanical stimulation.

**Acknowledgments** We would like to express gratitude to Professor Bin Li (Orthopedic Institute, Medical College, Soochow University) by providing the necessary materials, devices, and professional instructions. This study was supported by grants from the National Natural Science Foundation of China (31700854, 81771343, and 81471277), the Key Program of Anhui Province Educational

Committee (KJ2018A1011 and KJ2019A0392), the Natural Science Foundation of Anhui Province (1908085MC90 and 2008085QH362), the Scientific Research Foundation of Bengbu Medical College (BYKY17118, BYKY18108, BYKY1848ZD, and BYKY2019039ZD), the Translational Medicine Key Projects of Bengbu Medical College (BYTM2019006 and BYTM2019012), the Scientific Research Innovation Team of Bengbu Medical College (BYKC201910), the Postgraduate Research Innovation Project of Bengbu Medical College (Byycx1827, Byycx1954, Byycx1956, and Byycx1929), and the National Training Programs of Innovation and Entrepreneurship for Undergraduate (201910367041 and S201910367023).

#### Compliance with ethical standard

**Conflict of interest** The authors declare that they have no conflict of interests.

**Ethics Statement** This study was approved by the ethics committee of the medical faculty of Bengbu Medical College (Approval Number No. 2019100).

#### References

1. Yurube T, Takada T, Suzuki T, Kakutani K, Maeno K, Doita M, et al. Rat tail static compression model mimics extracellular matrix metabolic imbalances of matrix metalloproteinases, aggrecanases, and tissue inhibitors of metalloproteinases in intervertebral disc degeneration. *Arthritis Res Ther*. 2012;14:R51.
2. Vergroesen PP, Kingma I, Emanuel KS, Hoogendoorn RJ, Welting TJ, van Royen BJ, et al. Mechanics and biology in intervertebral disc degeneration: a vicious circle. *Osteoarthritis Cartilage*. 2015;23:1057–70.
3. Martin BI, Deyo RA, Mirza SK, Turner JA, Comstock BA, Hollingworth W, et al. Expenditures and health status among adults with back and neck problems. *JAMA*. 2008;299:656–64.
4. Bhunia BK, Kaplan DL, Mandal BB. Silk-based multilayered angle-ply annulus fibrosus construct to recapitulate form and function of the intervertebral disc. *Proc Natl Acad Sci U S A*. 2018;115:477–82.
5. Wan Y, Feng G, Shen FH, Laurencin CT, Li X. Biphasic scaffold for annulus fibrosus tissue regeneration. *Biomaterials*. 2008;29:643–52.
6. Zhu C, Li J, Liu C, Zhou P, Yang H, Li B. Modulation of the gene expression of annulus fibrosus-derived stem cells using poly(ether carbonate urethane)urea scaffolds of tunable elasticity. *Acta Biomater*. 2016;29:228–38.
7. Yang J, Yang X, Wang L, Zhang W, Yu W, Wang N, et al. Biomimetic nanofibers can construct effective tissue-engineered intervertebral discs for therapeutic implantation. *Nanoscale*. 2017;9:13095–103.
8. Du L, Yang Q, Zhang J, Zhu M, Ma X, Zhang Y, et al. Engineering a biomimetic integrated scaffold for intervertebral disc replacement. *Mater Sci Eng C Mater Biol Appl*. 2019;96:522–9.
9. Liu C, Zhu C, Li J, Zhou P, Chen M, Yang H, et al. The effect of the fibre orientation of electrospun scaffolds on the matrix production of rabbit annulus fibrosus-derived stem cells. *Bone Res*. 2015;3:15012.
10. Li Z, Lang G, Chen X, Sacks H, Mantzur C, Tropp U, et al. Polyurethane scaffold with in situ swelling capacity for nucleus pulposus replacement. *Biomaterials*. 2016;84:196–209.
11. Cortes DH, Han WM, Smith LJ, Elliott DM. Mechanical properties of the extra-fibrillar matrix of human annulus fibrosus are location and age dependent. *J Orthop Res*. 2013;31:1725–32.

12. Huang YC, Hu Y, Li Z, Luk KDK. Biomaterials for intervertebral disc regeneration: current status and looming challenges. *J Tissue Eng Regen Med*. 2018;12:2188–202.
13. Xu B, Du L, Zhang J, Zhu M, Ji S, Zhang Y, et al. Circumferentially oriented microfiber scaffold prepared by wet-spinning for tissue engineering of annulus fibrosus. *RSC Adv*. 2015;5:42705–13.
14. Martin JT, Milby AH, Chiaro JA, Kim DH, Hebel NM, Smith LJ, et al. Translation of an engineered nanofibrous disc-like angle-ply structure for intervertebral disc replacement in a small animal model. *Acta Biomater*. 2014;10:2473–81.
15. Abbott RD, Howe AK, Langevin HM, Iatridis JC. Live free or die: stretch-induced apoptosis occurs when adaptive reorientation of annulus fibrosus cells is restricted. *Biochem Biophys Res Commun*. 2012;421:361–6.
16. van Uden S, Silva-Correia J, Correlo VM, Oliveira JM, Reis RL. Custom-tailored tissue engineered polycaprolactone scaffolds for total disc replacement. *Biofabrication*. 2015;7:015008.
17. Saggese T, Teixeira GQ, Wade K, Moll L, Ignatius A, Wilke HJ, et al. GEORG SCHMORL PRIZE OF THE GERMAN SPINE SOCIETY (DWG) 2018: combined inflammatory and mechanical stress weakens the annulus fibrosus: evidences from a loaded bovine AF organ culture. *Eur Spine J*. 2019;28:922–33.
18. Pirvu T, Blanquer SB, Benneker LM, Grijpma DW, Richards RG, Alini M, et al. A combined biomaterial and cellular approach for annulus fibrosus rupture repair. *Biomaterials*. 2015;42:11–9.
19. Li L, Song K, Chen Y, Wang Y, Shi F, Nie Y, et al. Design and Biophysical Characterization of Poly (l-Lactic) Acid Microcarriers with and without Modification of Chitosan and Nanohydroxyapatite. *Polymers (Basel)*. 2018;10:1061.
20. Zhao Y, Liu B, Bi H, Yang J, Li W, Liang H, et al. The degradation properties of MgO Whiskers/PLLA composite in vitro. *Int J Mol Sci*. 2018;19:2740.
21. Stölzel K, Schulze-Tanzil G, Olze H, Schwarz S, Feldmann EM, Rotter N. Immortalised human mesenchymal stem cells undergo chondrogenic differentiation in alginate and PGA/PLLA scaffolds. *Cell Tissue Bank*. 2015;16:159–70.
22. Karimi Z, Seyedjafari E, Mahdavi FS, Hashemi SM, Khojasteh A, Kazemi B, et al. Baghdadite nanoparticle-coated poly l-lactic acid (PLLA) ceramics scaffold improved osteogenic differentiation of adipose tissue-derived mesenchymal stem cells. *J Biomed Mater Res A*. 2019;107:1284–93.
23. Vadalà G, Mozetic P, Rainer A, Centola M, Loppini M, Trombetta M, et al. Bioactive electrospun scaffold for annulus fibrosus repair and regeneration. *Eur Spine J*. 2012;21 Suppl 1:S20–6.
24. Li S, Jia X, Duance VC, Blain EJ. The effects of cyclic tensile strain on the organisation and expression of cytoskeletal elements in bovine intervertebral disc cells: an in vitro study. *Eur Cell Mater*. 2011;21:508–22.
25. Sen S, Jacobs NT, Boxberger JI, Elliott DM. Human annulus fibrosus dynamic tensile modulus increases with degeneration. *Mech Mater*. 2012;44:93–8.
26. Hee HT, Zhang J, Wong HK. Effects of cyclic dynamic tensile strain on previously compressed inner annulus fibrosus and nucleus pulposus cells of human intervertebral disc-an in vitro study. *J Orthop Res*. 2010;28:503–9.
27. Gilbert HT, Hoyland JA, Millward-Sadler SJ. The response of human annulus fibrosus cells to cyclic tensile strain is frequency-dependent and altered with disc degeneration. *Arthritis Rheum*. 2010;62:3385–94.
28. Zhou P, Chu G, Yuan Z, Wang H, Zhang W, Mao Y, et al. Regulation of differentiation of annulus fibrosus-derived stem cells using heterogeneous electrospun fibrous scaffolds. *J Orthop Translat*. 2020. <https://doi.org/10.1016/j.jot.2020.02.003>.
29. Fu Y, Liu L, Cheng R, Cui W. ECM decorated electrospun nanofiber for improving bone tissue regeneration. *Polymers (Basel)*. 2018;10:272.
30. Guo Q, Zhou P, Li B. Identification and characterizations of annulus fibrosus-derived stem cells. *Methods Mol Biol*. 2018;1842:207–16.
31. Chu G, Yuan Z, Zhu C, Zhou P, Wang H, Zhang W, et al. Substrate stiffness- and topography-dependent differentiation of annulus fibrosus-derived stem cells is regulated by Yes-associated protein. *Acta Biomater*. 2019;92:254–64.
32. Chu G, Zhang W, Zhou P, Yuan Z, Zhu C, Wang H, et al. Substrate topography regulates differentiation of annulus fibrosus-derived stem cells via CAV1-YAP-mediated mechanotransduction. *ACS Biomater Sci Eng*. 2020. <https://doi.org/10.1021/acsbiomaterials.9b01823>.
33. Uda Y, Azab E, Sun N, Shi C, Pajevic PD. Osteocyte Mechanobiology. *Curr Osteoporos Rep*. 2017;15:318–25.
34. Betti BF, Everts V, Ket JCF, Tabeian H, Bakker AD, Langenbach GE, et al. Effect of mechanical loading on the metabolic activity of cells in the temporomandibular joint: a systematic review. *Clin Oral Investig*. 2018;22:57–67.
35. Shradhanjali A, Riehl BD, Lee JS, Ha L, Lim JY. Enhanced cardiomyogenic induction of mouse pluripotent cells by cyclic mechanical stretch. *Biochem Biophys Res Commun*. 2017;488:590–5.
36. Tomlinson RE, Li Z, Li Z, Minichiello L, Riddle RC, Venkatesan A, et al. NGF-TrkA signaling in sensory nerves is required for skeletal adaptation to mechanical loads in mice. *Proc Natl Acad Sci U S A*. 2017;114:E3632–41.
37. Chen J, Wu X. Cyclic tensile strain promotes chondrogenesis of bone marrow-derived mesenchymal stem cells by increasing miR-365 expression. *Life Sci*. 2019;232:116625.
38. Sztrolovics R, Alini M, Roughley PJ, Mort JS. Aggrecan degradation in human intervertebral disc and articular cartilage. *Biochem J*. 1997;326:235–41.
39. Suna G, Wojakowski W, Lynch M, Barallobre-Barreiro J, Yin X, Mayr U, et al. Extracellular matrix proteomics reveals interplay of aggrecan and aggrecanases in vascular remodeling of stented coronary arteries. *Circulation*. 2018;137:166–83.

**Publisher's Note** Springer Nature remains neutral with regard to jurisdictional claims in published maps and institutional affiliations.